




Subaqueous landslide-triggered tsunami hazard for Lake Zurich, Switzerland

Michael Strupler^{1,3}  · Michael Hilbe² · Katrina Kremer³ · Laurentiu Danciu³ · Flavio S. Anselmetti² · Michael Strasser^{4,1} · Stefan Wiemer³

Received: 20 September 2017 / Accepted: 7 March 2018 / Published online: 14 March 2018
© Swiss Geological Society 2018

Abstract

Subaqueous landslides can induce potentially damaging tsunamis. Tsunamis are not restricted to the marine environment, but have also been documented on lakes in Switzerland and worldwide. For Lake Zurich (central Switzerland), previous work documented multiple, assumedly earthquake-triggered landslides. However, no information about past tsunamis is available for Lake Zurich. In a back-analysis, we model tsunami scenarios as a consequence of the earthquake-triggered landslides in the past. Furthermore, on the basis of a recent map of the earthquake-triggered subaqueous landslide hazard, we present results of a tsunami hazard assessment. The subaqueous landslide progression, wave propagation and inundation are calculated with a combination of open source codes. Although no historic evidence of past tsunamis has been documented for Lake Zurich, a tsunami hazard exists. However, only earthquakes with long return periods are assumed to cause considerable tsunamis. An earthquake with an exceedance probability of 0.5% in 50 years (corresponding to an earthquake with a return period of 9975 years) is assumed to cause tsunamigenic landslides on most lateral slopes of Lake Zurich. A hypothetical tsunami for such an event would create damage especially along the shores of the central basin of Lake Zurich with estimated peak flow depths of up to ~ 4.6 m. Our results suggest that for an earthquake with an exceedance probability of 10% in 50 years (i.e., mean return period of 475 years), no considerable tsunami hazard is estimated. Even for a worst-case scenario, the cities of Zurich and Rapperswil, located at the northern and southern ends of the lake, respectively, are assumed to experience very little damage. The presented first-order results of estimated wave heights and inundated zones provide valuable information on tsunami-prone areas that can be used for further investigations and mitigation measures.

Keywords Subaqueous mass movements · Tsunami hazard assessment · Tsunami modelling · Lake Zurich

Editorial handling: D. Aritztegui.

Electronic supplementary material The online version of this article (<https://doi.org/10.1007/s00015-018-0308-5>) contains supplementary material, which is available to authorized users.

✉ Michael Strupler
michael.strupler@erdw.ethz.ch

¹ Geological Institute, ETH Zurich, Sonneggstrasse 5, 8092 Zurich, Switzerland

² Institute of Geological Sciences and Oeschger Centre for Climate Change Research, University of Bern, Bern, Switzerland

³ Swiss Seismological Service, ETH Zurich, Zurich, Switzerland

⁴ Institute of Geology, University of Innsbruck, Innsbruck, Austria

1 Introduction

1.1 Background

Subaqueous landslides can be triggered by different mechanisms, e.g. earthquakes, wave loading, water-level changes, sediment overloading, or fluid escape (e.g. Locat and Lee 2002). In many cases, such subaqueous landslides occur without anybody's awareness (Lee et al. 1993). In some cases, however, subaqueous landslides may induce tsunamis (i.e., gravity-driven water waves), that potentially cause damage to civilisation and coastal infrastructure (e.g. Jiang and Leblond 1992; Tappin 2017). The height of landslide-generated waves depends primarily upon the volume of the mass movement, its initial acceleration, speed, water depth and coherence (Watts 1998; Tappin

et al. 2008; Bornhold and Thomson 2012). A subaqueous landslide typically creates waves that travel both in the direction of the slide and opposite to the slide (Tinti and Bortolucci 2000). The impact of tsunamis on the shores can be described by the run-up (i.e. the vertical distance between the sea-/lake level at rest and maximum height reached by the tsunami on the shore), the inundation distance and inundation area (i.e. horizontal distance and area that a tsunami penetrates inland, respectively) and flow depth (i.e. the water depth during inundation on land) (Pararas-Carayannis 1988; Intergovernmental Oceanographic Commission 2016). Most of the tsunami waves do not break, they rather flow like a river on the shores (Pelínovsky and Mazova 1992; Ward 2011).

Well-investigated examples of past tsunamis resulting from earthquake-triggered landslides include the 8150 BP Storegga landslide tsunami (e.g. Harbitz 1992; Bondevik et al. 2005; Løvholt et al. 2005; Hill et al. 2014), the 1929 AD Grand Banks landslide tsunami (Fine et al. 2005; ten Brink et al. 2009), and the 1998 AD Papua New Guinea tsunami (Tappin et al. 1999, 2001; Synolakis et al. 2002). Modelling of assumedly earthquake-triggered subaqueous landslides also allowed the investigation of past tsunamis in New Zealand (Wang et al. 2016) and Puerto Rico (López-Venegas et al. 2008). Previous work suggested that earthquakes have repeatedly caused multiple subaqueous landslides on the slopes of Swiss perialpine lakes (e.g. Schnellmann et al. 2002; Strasser et al. 2013; Kremer et al. 2014; Reusch et al. 2016). Some of these slides were even related to historically reported tsunamis in Lake Lucerne (Siegenthaler et al. 1987; Schnellmann et al. 2002), which were reproduced with numerical modelling by Hilbe and Anselmetti (2015). The latter study combined publicly available codes for modelling mass movements, wave generation, propagation, and inundation to simulate historically reported and hypothetical tsunamis in Lake Lucerne. Peak wave heights and maximum run-up of several meters on the shores of Lake Lucerne were estimated.

For Lake Zurich, reflection seismic and bathymetric datasets (Schlund 1972; Strasser et al. 2013; Strupler et al. 2015) show fingerprints of many postglacial subaqueous mass movements affecting the lateral slopes. Three major basin-wide lateral slope-failure events (dated to ~ 2210 , ~ 11600 and ~ 13760 cal. year BP) were interpreted by Strasser et al. (2013) as earthquake-triggered, due to the synchronous occurrence of multiple slides in the lake basin (i.e., they appear on the same seismic stratigraphic horizon and are therefore considered coeval). It is not known whether tsunamis occurred as a consequence of these events, but it was hypothesized that the event ~ 13760 cal. year BP might have triggered a tsunami (Strasser et al. 2008). For various human-triggered slides that occurred in the last 150 years on the lateral slopes of

Lake Zurich (Heim 1876; Nipkow 1927; Kelts and Hsü 1980; Kuen 1999), no tsunami waves have been reported. However, documented evidence of past landslides, as well as potentially unstable slopes that have been mapped for different earthquake hazard levels (Strupler et al. 2018) highlight the need to assess the tsunamigenic potential of past and potential future subaqueous slope failures.

1.2 Objectives

This study presents a first-order tsunami-hazard assessment that follows up on the assessment of the earthquake-triggered subaqueous landslide hazard (Strupler et al. 2018). The aims of this study are (a) to investigate the tsunamigenic potential of past subaqueous landslides on the lateral slopes of Lake Zurich, and (b) to assess the hazard of tsunamis related to potential future earthquake-triggered landslides in the study area. With the approach of Hilbe and Anselmetti (2015) and the model limitations described therein, the impact of different landslide scenarios are modelled in terms of peak wave height, onshore flow depth and inundation:

- The past tsunamigenic potential is investigated for an event of multiple basin-wide, assumedly earthquake-triggered landslides that occurred ~ 2210 cal. year BP at the slopes of Lake Zurich (Strasser et al. 2013). From the three major events documented by Strasser et al. (2013), the ~ 2210 cal. year BP event is selected for a back-calculation of the landslide characteristics, based on the extent of the deposit. That event is selected, as it occurred on the lateral slopes with the same lithostratigraphic succession as today's undisturbed slopes (due to its relatively younger age compared to the other events). Because of the same lithostratigraphic succession at the time of that event, similar landslide-mobility parameters are expected for the present conditions.
- The current tsunami hazard is assessed by simulating the consequences of basin-wide slope failures that are to be expected (Strupler et al. 2018) for earthquake accelerations with a probability of exceedance in 50 years (EP_{50}) of 10, 2 and 0.5% (i.e., mean return periods of 475, 2475 and 9975 years, respectively).

2 Setting of the study area and previous studies

2.1 Study area

Lake Zurich ($\sim 47^\circ\text{N}$, 8.5°E , 406 m a.s.l.) is located in a glacially overdeepened trough in northern Switzerland. Remnants of a recessional terminal moraine from the last

glaciation separate Lake Zurich in two parts (e.g. Keller and Krayss 2005; Fig. 1). The part to the northwest of the moraine is termed Lake Zurich *sensu stricto*, and the part to the southeast of the moraine is termed Obersee. The northern part of Lake Zurich consists of a shallow zone near the city of Zurich, Switzerland's economic capital, followed by an up to 136 m deep, central basin and an again shallow (~ 25 m), flat southeastern basin, which hosts two islands 'Ufenau' and 'Lützelau' with highest elevations of 17 and 8 m above lake level, respectively. The central basin and the southeastern basin are connected via an escarpment structure with topographic steps in the Molasse bedrock. The main tributaries are the Linth, Jona and Wägitaler Aa rivers. The only outflow is the Limmat River at the northern end of the lake. Today, the lake level is managed and in the recent years, the mean monthly lake level fluctuated between ~ 405.6 and ~ 406.5 m a.s.l. (AWEL 2016).

The majority of the documented subaqueous landslides occurred on the lateral slopes surrounding Lake Zurich's central basin (Strasser et al. 2013; Strupler et al. 2015). Relatively recent subaqueous slides (i.e., in the last 150 years) occurred offshore the villages of Horgen, Oberrieden, Rüslikon and Küsnacht (Fig. 1; Heim 1876; Nipkow 1927; Kelts and Hsü 1980; Kuen 1999). The

shores of Lake Zurich are densely populated, approximately a quarter million people live within 1 km from the lakeshore, and ~ 57,000 of these live less than 10 m above lake level (Henriod et al. 2016).

2.2 Previous studies

Strupler et al. (2017) categorized the post-glacial lithological succession on the lateral slopes of Lake Zurich into four sediment-mechanical units, based on characteristic patterns of bulk density (ρ_{bulk}) and undrained shear strength (s_u). The same study investigated the glide planes of three subaqueous landslides, located offshore Oberrieden (Fig. 1), which are assumed to have occurred in water-saturated sediments under undrained conditions. All the glide planes lie within a sediment-mechanical unit with relatively high ρ_{bulk} , but low s_u , corresponding to a lithological unit consisting of Late Glacial plastic muds.

A recent study by Strupler et al. (2018) assessed the earthquake-triggered, subaqueous landslide hazard by conducting a spatially distributed slope-stability analysis that considered earthquake accelerations from a probabilistic seismic hazard assessment (Wiemer et al. 2016). These authors calculated slope stabilities for all cells of an equally-spaced grid with a limit-equilibrium equation on an

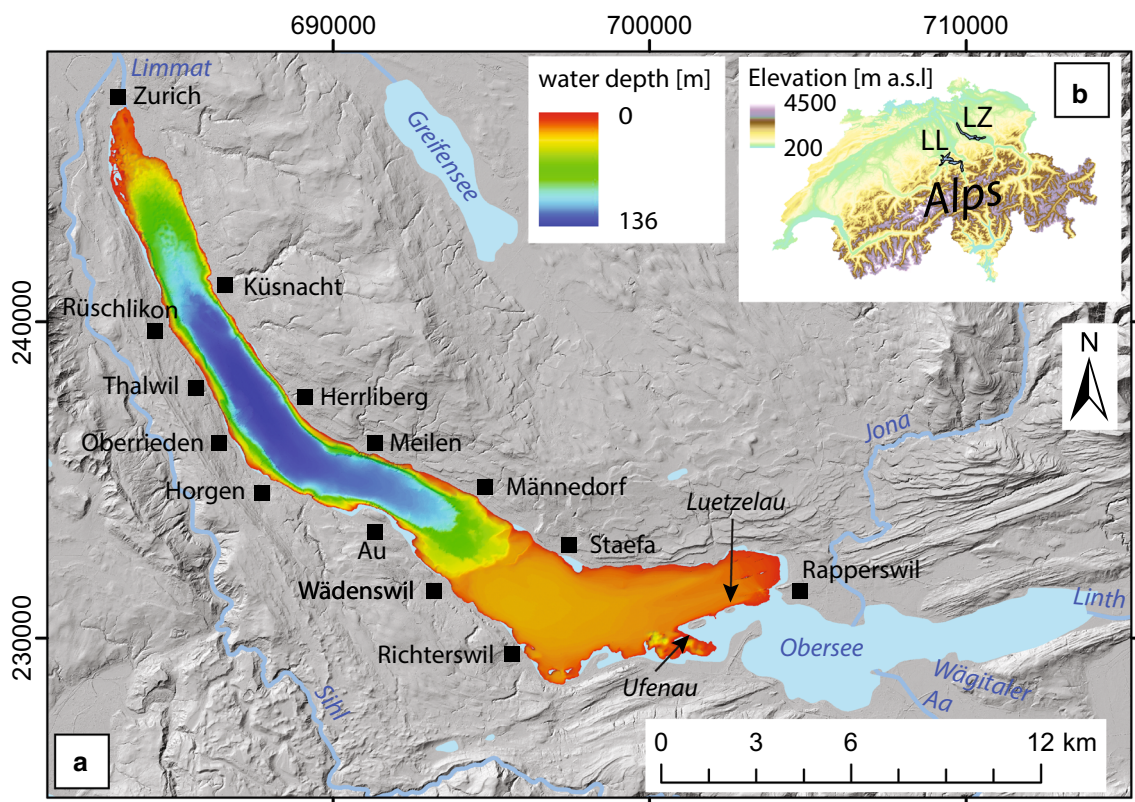


Fig. 1 a Map of the study area. LiDAR digital elevation model and surface water data from Swisstopo. Bathymetric dataset from Strupler et al. 2015. Swiss coordinates (LV03). b Location of the study lake within Switzerland. LZ Lake Zurich, LL Lake Lucerne

infinite slope. The thickness of the sediment-mechanical units at each pixel location was estimated as a function of water depth and slope gradient, calculated with a sedimentation model (Strupler et al. 2018). Profiles of ρ_{bulk} and s_u vs. depth were adapted to the thickness of the sediment-mechanical units at each pixel. Random values from log-normally distributed ρ_{bulk} and s_u profiles were selected for each depth step with a Monte Carlo Simulation, to incorporate uncertainty due to the spatial variability of the sediment-mechanical data.

Earthquake shaking was implemented as pseudostatic acceleration, which was assumed to represent 50% of the peak ground acceleration (PGA). For each pixel of the bathymetric dataset of Lake Zurich (Strupler et al. 2015), a probability of failure (conditional on earthquake shaking; PoF_{eo}) vs. depth profile was calculated.

In that model, the glide plane was defined as the depth of the maximum PoF_{eo} (queried from the top of the PoF_{eo} vs. depth profile). Mean PGAs for earthquakes with EP_{50} of 10, 2 and 0.5% (corresponding to mean return periods of 475, 2475 and 9975 years, respectively) from a probabilistic seismic hazard analysis (Wiemer et al. 2016) were considered for the earthquake-triggered landslide hazard assessment.

Strupler et al. (2018) mapped individual slopes with high PoF_{eo} (i.e., > 0.6 ; Fig. 2). While for an earthquake with an EP_{50} of 10% (median PGA: ~ 0.05 g) only minor parts of the slopes are expected to fail (cumulative slide volume of ~ 3 Mio m^3 ; Fig. 2), for an earthquake with an EP_{50} of 2% (median PGA ~ 0.1 g), larger parts are expected to slide downslope (cumulative slide volume of ~ 12 Mio m^3), and for an earthquake with an EP_{50} of 0.5% (median PGA: ~ 0.2 g), most of the yet unfailed, lateral slopes are expected to become unstable (i.e., cumulative slide volume of 48 Mio m^3 , excluding slopes $< 1^\circ$, to avoid large instable volumes on the terraces of the escarpment structure; Strupler et al. 2018).

Because the model of Strupler et al. (2018) defines the glide plane as the depth of the maximum PoF_{eo} , the slide thickness is occasionally a few dm lower for a scenario of an EP_{50} of 0.5% compared to an EP_{50} of 2%. Hence, the higher earthquake acceleration for an EP_{50} of 0.5% causes the slope to fail a few dm higher (Fig. 2).

Hilbe and Anselmetti (2015) modelled the kinematics of subaqueous landslides in Lake Lucerne (Fig. 1b) as single-phase, fluid-like mass movements propagating on the lake floor with MassMov2D (Beguiría et al. 2009), which is implemented in the free GIS package PCRaster (Wesseling et al. 1996). Hilbe and Anselmetti (2015) fed the output of MassMov2D (i.e., the changing bathymetry as a function of time) into GeoClaw (Berger et al. 2011) in order to calculate wave generation, propagation and inundation, starting with a lake surface at rest. The results of the numerical

experiments performed on Lake Lucerne showed a good agreement with historically reported tsunami effects. However, according to Hilbe and Anselmetti (2015), the model likely overestimates wave heights and run-up close to the tsunami source areas, which is an important limitation.

3 Data and methods

The mass-movement propagation was simulated in a first step, followed by modelling the tsunami wave generation and propagation as in Hilbe and Anselmetti (2015). Calculations were done with a grid resolution of 20 m. Previous sensitivity tests demonstrated that smaller grid sizes do not have a significant influence on runout distance, velocity and geometry of the deposit for the mobility analysis of the landslide, and the amplitudes of the free surface wave do not significantly change for a smaller grid size (Hilbe and Anselmetti 2015).

3.1 Simulation of the subaqueous landslide progression

The MassMov2D program code, used for the landslide simulation, needs a digital terrain model (DTM) as input. For the study area, this DTM was created by combining a digital elevation model (DEM), which was resampled from a grid resolution of 2 m (SwissAlti3D; swisstopo) to 20 m and a digital bathymetric model (DBM). The DBM was interpolated from isobaths of the swiss digital height model DHM25 that shows digitised height information of the 1:25,000 national map (swisstopo). For the modelling of landslides and tsunamis, we did not consider an available high-resolution DBM (Strupler et al. 2015) because all the calculations were conducted on a 20 m resolution and also to reduce computing time.

3.1.1 Thickness of the mobile sediment drape and rheological input parameters

The back-calculated (in the case of the ~ 2210 cal. year BP Oberrieden event) and estimated slide volumes for potential future earthquakes with their respective EP_{50} are taken from Strupler et al. (2018). In contrast to Hilbe and Anselmetti (2015), who assumed a constant thickness for the slides, Strupler et al. (2018) assume slightly varying slide thicknesses within the slides. This variation in thickness comes from the fact that the authors model the sediment-thickness on the slopes as a function of slope gradient and water depth for each pixel.

After adding the initial slide thicknesses to the DBM, the subaqueous landslide is modelled with the Bingham

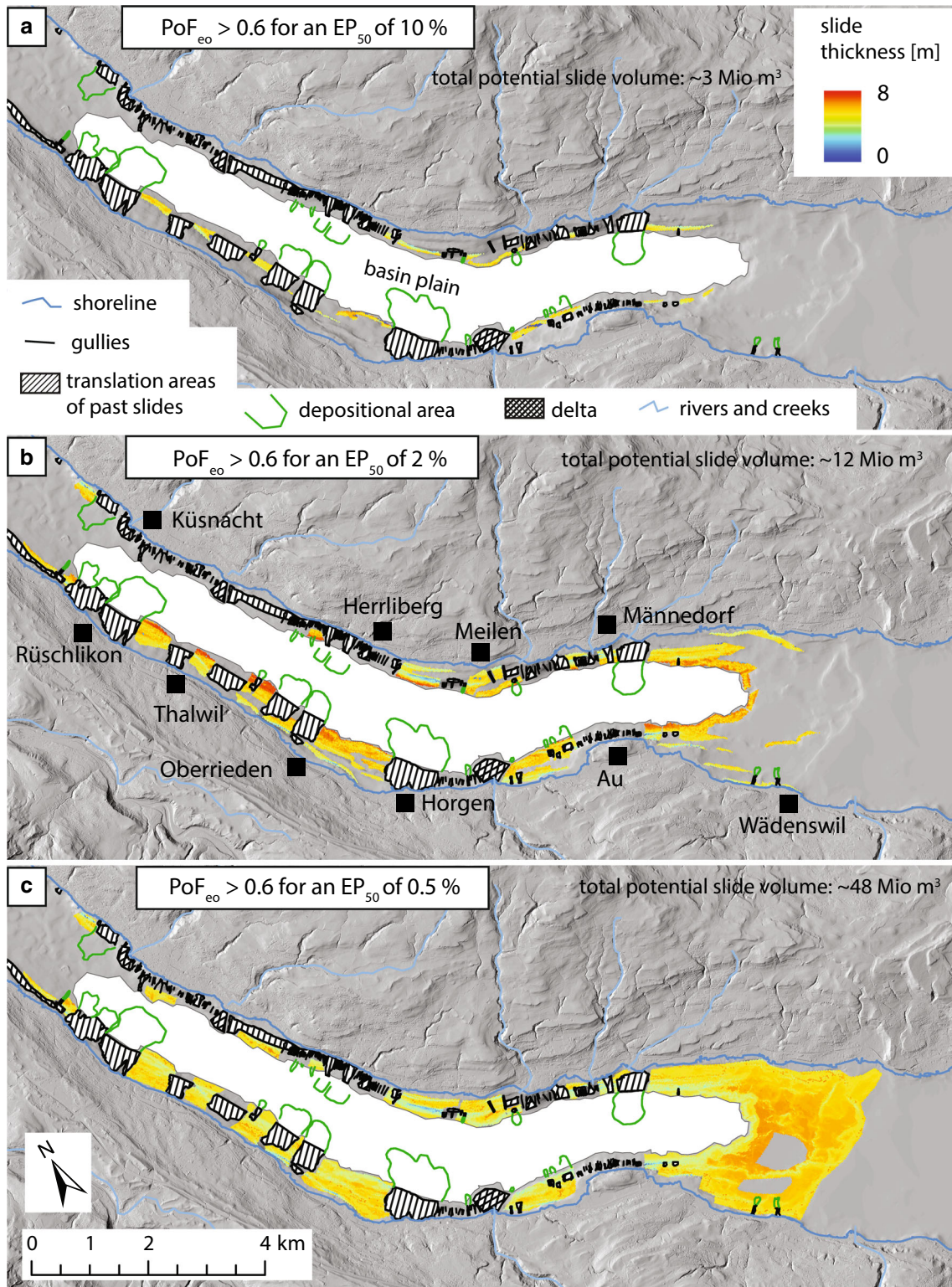


Fig. 2 Zones with a high failure probability upon earthquake occurrence (PoF_{eo}) and corresponding potential failure depths for peak ground accelerations with an exceedance period in 50 years of **a** 10%, **b** 2% and **c** 0.5% (Strupler et al. 2018). Slopes $< 1^\circ$ are here

considered stable (to avoid large unstable volumes on the terraces of the escarpment structure), although the model of Strupler et al. (2018) considers such slopes (i.e., $> 0.01^\circ$ – 1°) as unstable for strong earthquake accelerations, such as assumed for an EP_{50} of 0.5%

plastic rheology, as mud-rich subaqueous sediments behave approximately as Bingham plastic fluids (e.g. Mei and Liu 1987; Skvortsov and Bornhold 2007). As rheological input parameters, submerged bulk density ρ' [kg m^{-3}], dynamic viscosity μ [Pa s], and yield strength τ [Pa] are required. We assumed a submerged bulk density of $\rho' = 600 \text{ kg m}^{-3}$, which corresponds to the typical bulk of the Late Glacial plastic muds, the unit in which the glide plane is located (Strupler et al. 2017), minus the density of the ambient water. The parameters μ and τ were calibrated on the distinct slide deposit of the ~ 2210 cal. year BP Oberrieden slide (Strupler et al. 2015) by matching the modelled landslide runout with the observed extent of the deposition lobe. Subsequently, these parameters were used for the calculation of all the slide scenarios (see Sect. 4.1.1).

3.2 Tsunami wave propagation modelling and flow depth

The propagation of the tsunami wave, as well as the inundation, were calculated with the GeoClaw code (version 4.6.3; Berger et al. 2011). The peak wave height was recorded on virtual gauges that were defined in the study area (Table 1):

The DTM does not include buildings or vegetation, which could drag the tsunami wave and thus reduce the inundated area. Friction is implemented in the GeoClaw code by applying a Manning roughness coefficient. The Manning coefficient can vary from ~ 0.015 for very smooth terrain to ~ 0.07 very rough coastal areas (Bretschneider and Wybro 1977). Here, as Hilbe and Anselmetti (2015), we apply a coefficient of 0.03 (representing grass, roads, and scrubs; e.g. Kaiser et al. 2011).

Previous lake-level reconstructions (based on the evidence on lacustrine chalks above the present lake level) suggest a ~ 2 m higher lake level between the first millennium BC and the first century AD, caused by damming of the lake outflow by sediments of the Sihl River (Wild

2009). Therefore, the lake level was set to 408 m for the back-analysis of the free surface wave height, flow depth and inundated area of a potential ~ 2210 cal. year BP tsunami. The present-day lake level of 406 m was used for the assessment of the current tsunami hazard.

4 Results

4.1 Mobility analysis of past and potential future mass movements

In this section, we provide results of landslide-mobility analyses for (i) the single ~ 2210 cal. year BP subaqueous slide offshore Oberrieden (Sect. 4.1.1), (ii) for the case of all ~ 2210 cal. year BP slides occurring simultaneously (Sect. 4.1.2), and (iii) for hypothesized landslides assumed to be triggered by PGAs with EP_{50} of 10, 2 and 0.5% (Sect. 4.1.3).

4.1.1 Back-analysed scenario Oberrieden ~ 2210 cal. year. BP

The following input parameters were back-analysed from the 2210 cal. year. BP Oberrieden slide (Table 2).

The rheological parameters μ and τ were iteratively varied to match the slide extent. For $\mu = 40 \text{ Pa s}$ and $\tau = 5 \text{ Pa}$, the modelled runout of the ~ 2210 cal. year BP Oberrieden slide shows a relatively good agreement with the toe of the observed landslide deposit (ESM Fig. 1).

Table 2 Back-analysed parameters for the ~ 2210 cal. year. BP Oberrieden slide, used to model the forward scenarios

Rheological model	Bingham
Submerged bulk density ρ' [kg m^{-3}]	600
Yield strength τ [Pa]	5
Dynamic viscosity μ [Pa s]	40
Landslide propagation time [s]	120

Table 1 Gauge locations (Swiss grid coordinates LV03 in m) in the lake (see also Figs. 5, 6, and 8)

Gauge-Nr.	x-Coordinate	y-Coordinate	Location	Present-day water depth [m]
1	687315	237735	Central deep basin	136
2	688572	237571	Herrliberg harbour	14
3	686406	237293	Oberrieden	3
4	690935	235857	Meilen harbour	15
5	687716	235268	Horgen harbour	8
6	685553	238880	Thalwil harbour	12
7	683287	246640	Offshore Zurich Buerkliplatz	11
8	704081	231435	Rapperswil harbour	1
9	683819	244703	Northern basin	32
10	697195	231070	Southern basin	25

Both the modelled runout distance (i.e. the distance from the toe of the slope to the maximal extension of the deposit) and the measured runout distance of the deposit are 490 m. The modelled maximum width of the deposition lobe, however, is 780 m, compared to measured 560 m. The slide reaches a maximum speed of 14 m/s. 30 s after slide initiation, the speed of the slide is ~ 5 m/s. After ~ 90 s, the maximum extent of the slide is reached, and only minor movements within the depocenter are occurring (~ 1 m/s). The modelled deposit at its final stage has a maximum thickness of ~ 3 m. As in Hilbe and Anselmetti (2015), a thin layer remains in the source area. The authors interpreted this as an effect of the used Bingham plastic rheology. The modelled deposit thickness is much lower than the measured maximum deposit thickness in the seismic reflection dataset (~ 15 m; Strasser et al. 2013; Strupler et al. 2015). However, a considerable percentage of the latter is composed of deformed basin-floor sediments, which have not been transported from the source area of the landslide, but deformed virtually in place. This process is obviously not included in the landslide-mobility model. Due to the fact that the slide is modelled as a Bingham fluid, some lateral spreading occurs, making the modelled deposition zone slightly wider than the mapped one from Strupler et al. (2015).

4.1.2 Back-analysed scenario of multiple landslides dated to ~ 2210 cal. year BP slides

Strasser et al. (2013) assigned a total of ten individual landslide deposits to the assumedly earthquake-triggered ~ 2210 cal. year BP event. For some of these deposits, the corresponding source and translation areas could not be distinguished clearly because they have been overprinted by human-triggered slides in the last 150 years (Heim 1876; Nipkow 1927; Kelts and Hsü 1980; Kuen 1999). Due to the overprinting and the fact that the back-calculated depth of the glide plane for the ~ 2210 cal. year BP event is only available for the Oberrieden case-study site (Strupler et al. 2018), a constant depth to the glide plane of 5 m was assigned for the other ~ 2210 cal. year BP slides (mean headscarp heights ~ 3 – 7 m; Strupler et al. 2015). The translation area corresponding to the northernmost deposit with the smallest extent of the ~ 2210 cal. year BP event could not be identified in the bathymetric dataset (Strupler et al. 2015). It is assumed that this very small slide was draped by sediments from the Künsnacht Delta and is thus not included in the simulation of all ~ 2210 cal. year BP slides. The total volume of the slides assigned to the ~ 2210 cal. year BP event accounts to ~ 4 Mio m^3 , which is five times larger than the single ~ 2210 cal. year BP Oberrieden slide modelled above (Sect. 4.1.1; $803,900$ m^3 ; Strupler et al. 2018).

The modelled mass transport deposits (MTDs) of the ~ 2210 cal. year BP event on the western slopes coincide well with the extents of the MTDs mapped in Strasser et al. (2013). On the eastern slope, the modelled slides correlate only partly with the mapped extent of the deposits (Fig. 3). There is a relatively large discrepancy between the modelled and mapped MTDs from the seismic reflection data between the villages of Erlenbach and Herrliberg, which may be related to mapping uncertainties on these steep zones, where also many gullies occur (Strupler et al. 2015). Instead of two distinct deposits, such as mapped from the seismic reflection seismic data (Strasser et al. 2013), only one wider slide is modelled.

4.1.3 Potential future subaqueous slides for PGA of different EP_{50} scenarios

Results from a mobility analysis of subaqueous landslides that are assumed to occur as a consequence of different earthquake-hazard scenarios (Fig. 2; Strupler et al. 2018) provide the backbone for the current hazard assessment. Using the rheological parameters from the back-analysis of the ~ 2210 cal. year BP Oberrieden slide (Table 2), the distributions of the modelled basin-wide MTDs show greater runout distances for landslides triggered by stronger earthquakes (smaller EP_{50}) than for landslides triggered by weaker earthquakes (greater EP_{50}) (Fig. 4). Due to the fact that most failure-prone zones for earthquakes with an EP_{50} of 10% are located near the bottom of the slopes, the height drop (i.e. elevation difference between headscarp and farthest extent of the deposit) is small and the slope angles are low, implying slow velocities and short runout distances. Modelled thicknesses of the landslide deposits vary between ~ 1 and ~ 1.5 , between ~ 1 and ~ 4 , and between ~ 1 and ~ 10 m for potential landslides triggered by an earthquake with PGAs for an EP_{50} of 10, 2, and 0.5%, respectively (Fig. 4).

4.2 Simulation of landslide-induced tsunami waves

4.2.1 Back analysed potential tsunami caused by earthquake-triggered landslides ~ 2210 cal. year BP

The modelled simultaneous triggering of all the documented ~ 2210 cal. year BP slides (cumulative volume: ~ 4 km^3) causes the strongest tsunami effects alongshore the central basin. At the gauge located behind the Oberrieden slide, a peak amplitude of ~ 1.5 m is recorded (~ 1 min after slide initiation; Fig. 5). After that, the wave oscillates with peak amplitudes of ~ 0.5 m for the following 10 min. In Thalwil, three successive waves of

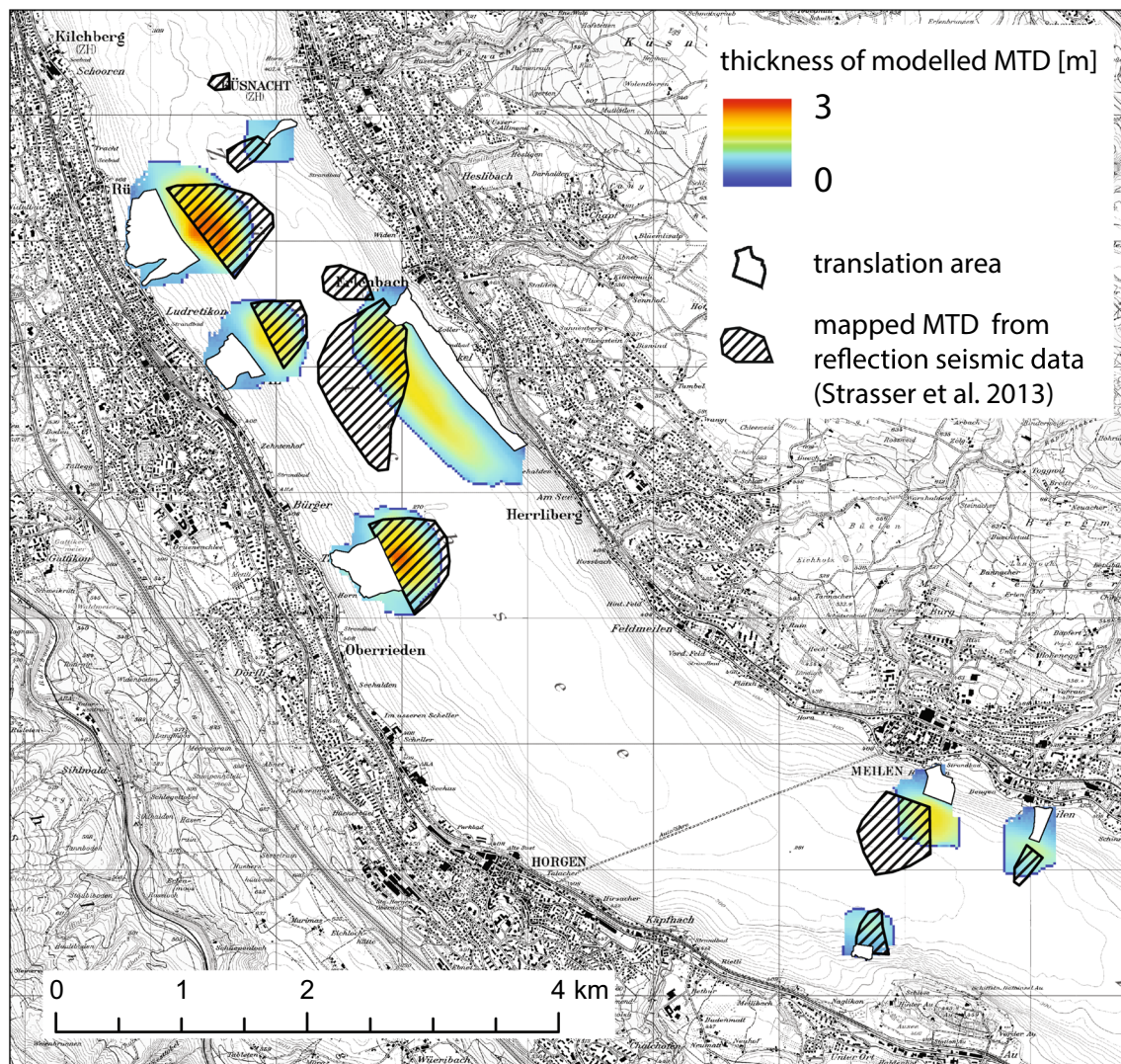


Fig. 3 Modelled mass transport deposits (MTD) from a mobility analysis of all ~ 2210 cal. year BP slides mapped in Strasser et al. (2013)

0.5–1 m peak amplitude arrive within the first 3 min after the triggering of the slides. After that, the waves diminish to half of their size, continuing for another 15 min. The first wave peak arrives at the northern end of Lake Zurich (offshore today's location of Buerkliplatz) ~ 8 min after the triggering of the landslides, with a low peak amplitude of ~ 0.1 m (ESM, Fig. 4). At the gauge location Rapperswil, a wave of only ~ 1 cm can be detected after ~ 15 min. In such a case of a synchronous sliding of all the 2210 cal. year BP events, the shorelines around the deep basin (mainly on the western lake shores in the near field of landslides; Fig. 5) may have experienced maximum flow depths of up to ~ 3 m under assumption of a paleolake level of 408 m a.s.l. with the present-day DTM (which may lead to overestimations of flow depths due to anthropogenic fillings along the shoreline).

4.2.2 Scenario for tsunamis caused by hypothetical landslides that may be triggered by earthquakes with a median PGA for an EP50 of 10 and 2%

The total slide volume of an earthquake with PGAs for an EP₅₀ of 10% that was estimated by Strupler et al. (2018) to ~ 3 Mio m³ (Fig. 2a), would cause free surface waves with maximum peak amplitudes of 0.4 m in the deep basin (Fig. 6a), given that all these slides occurred simultaneously. 5 min after slide initiation, the peak amplitudes do not exceed 0.2 m at all the gauges. This scenario does not cause any considerable inundation.

Estimated slope failures triggered by an earthquake with an EP₅₀ of 2% would lead to a similar pattern of tsunami occurrences as assumed for tsunamis caused by estimated slope failures triggered by earthquakes with an EP₅₀ of

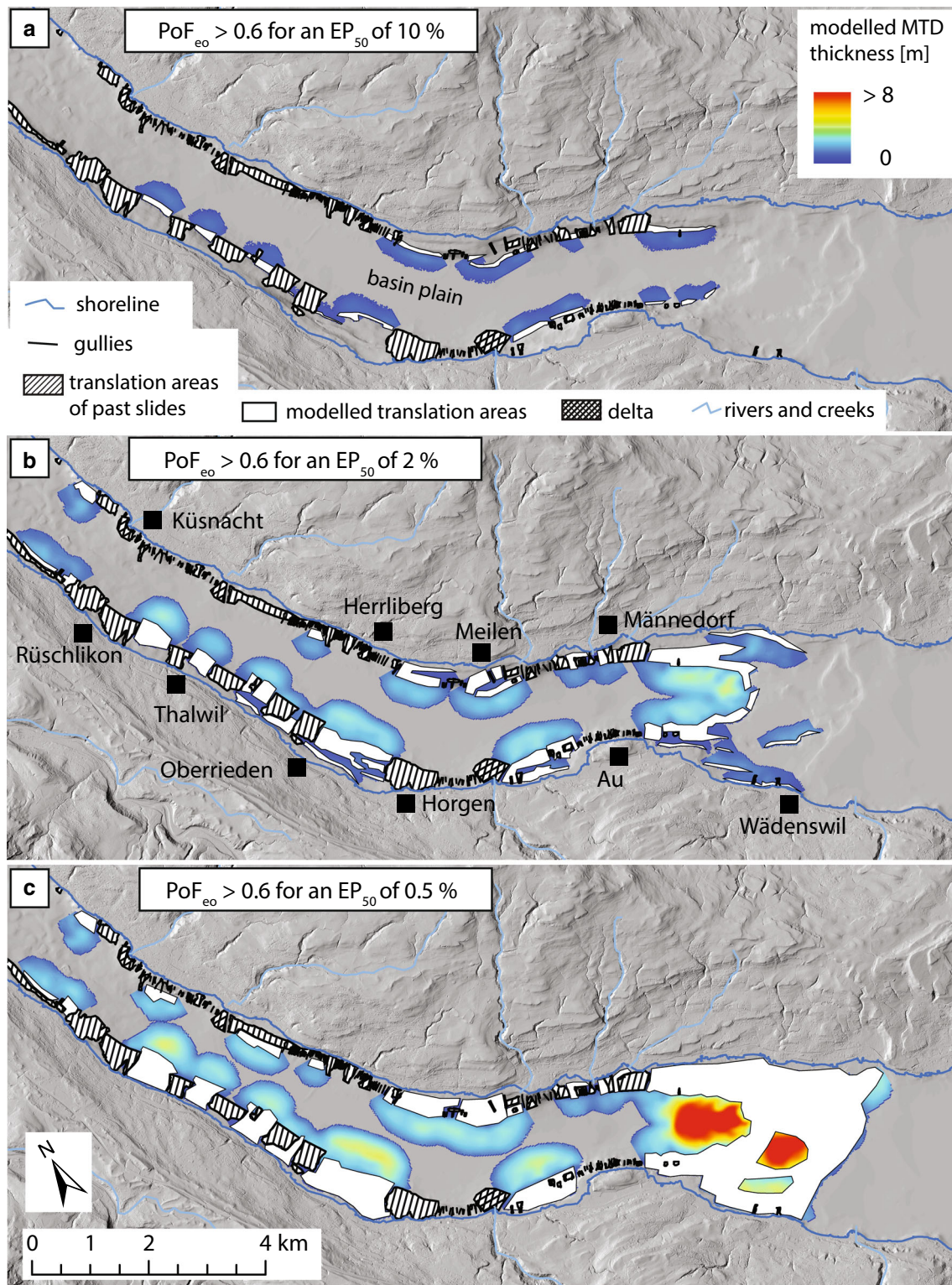


Fig. 4 Spatial distributions and thicknesses of mass transport deposits modelled for potential landslides expected for earthquake scenarios with different exceedance periods of **a** 10, **b** 2 and **c** 0.5% in 50 years

10%. The main difference is that the expected peak amplitudes are higher for an EP_{50} of 2% (instead of maximum peak amplitudes of ~ 0.4 m (Fig. 6a), they reach up

to ~ 2 m, albeit in the near field of the landslides; Fig. 6b). The shores around the deep basin would be inundated, e.g. south of Au and around the village of

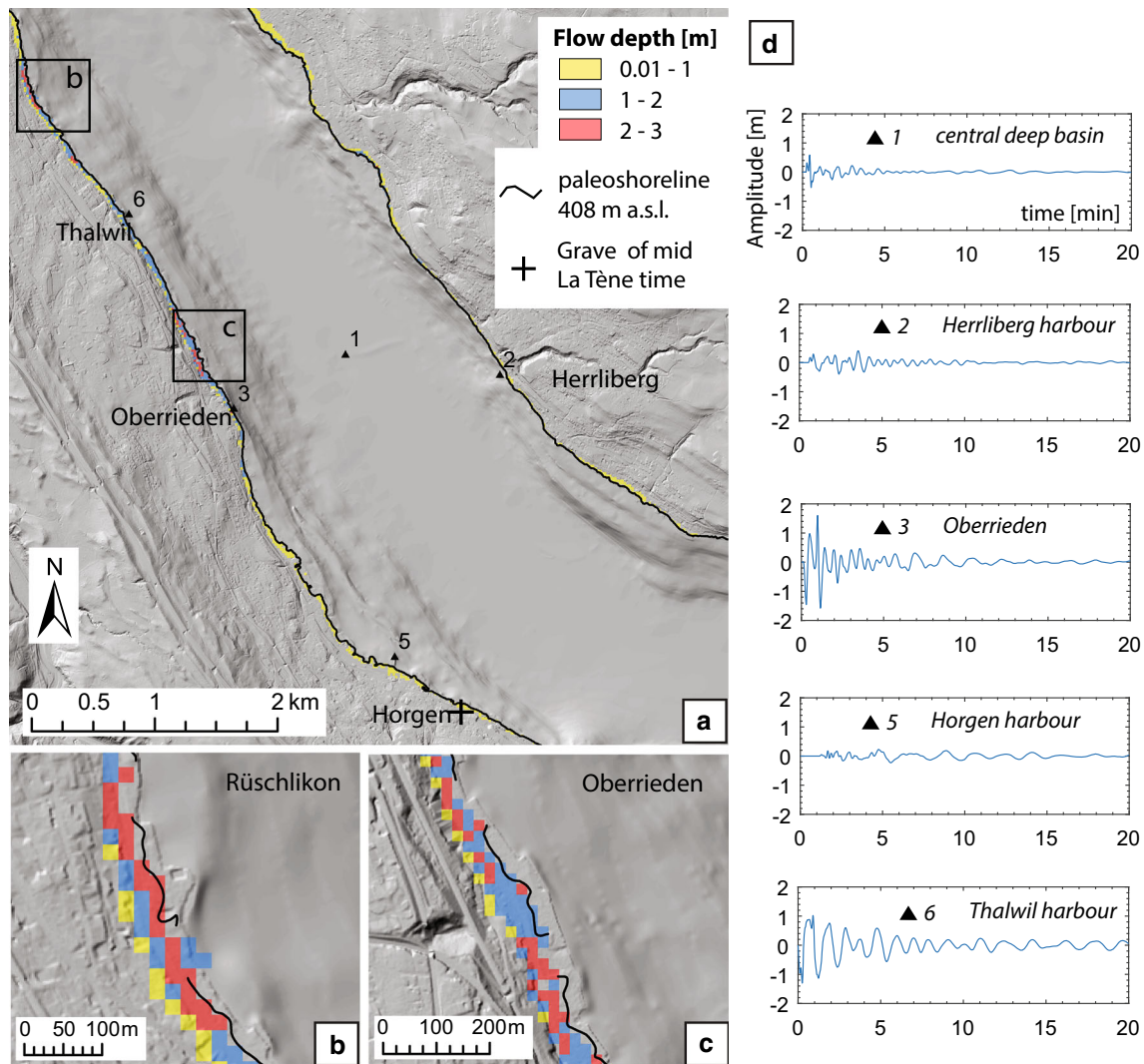


Fig. 5 a Back-analysed inundation and flow depth on the shores of the deep basin for a scenario of a coeval failure of all slides assigned to the ~ 2210 cal. year BP earthquake. b Zoom Rüslikon, c Zoom Oberrieden, d Time series of wave amplitudes at different gauges

Uetikon, the latter at the former location of the oldest Swiss chemical production site for fertilizer; Fig. 7; Geilinger-Schnorf 1993). However, the maximum flow depth would amount to less than 1 m for most zones.

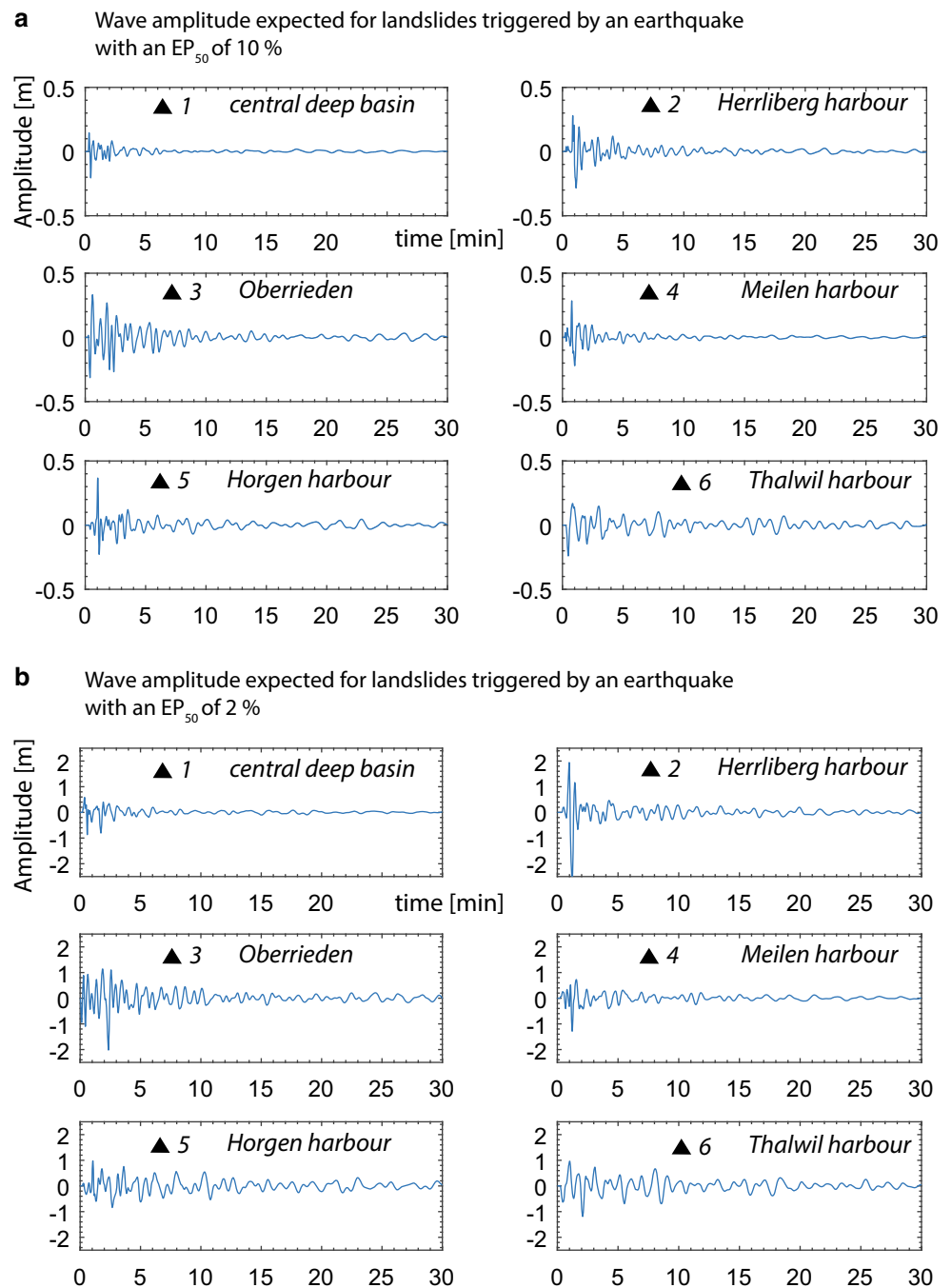
4.2.3 Scenario for tsunamis caused by hypothetical landslides that may be triggered by an earthquake with a median PGA expected for an EP_{50} of 0.5%

For a worst-case scenario of all yet unfailed slopes sliding down simultaneously (as expected for an earthquake with an EP_{50} of 0.5%; Strupler et al. 2018), the entire shoreline would be affected. The villages located around the central basin, where the majority of the slides occur, would especially be affected by inundations within the first 10 min after the occurrence of the slides. The most distal cities of Zurich and Rapperswil would be affected by the

tsunami only ~ 5 and ~ 12 min after the slide occurrence, respectively. In Zurich, after two initial waves with a peak elevation of ~ 0.5 m, the lake level would lower during ~ 3 min by ~ 2 m and rise again for the succeeding 3 min (gauge 7, Fig. 8). This irregular wave pattern has been interpreted to be caused by interference of the waves. For an earthquake with a mean return period of ~ 9975 years, large landslides occur between Meilen and Herrliberg, causing initial peak amplitudes of more than ~ 2 m measured at the nearby virtual gauges 2 and 4 (Fig. 8).

The zones most affected by inundation on the western shores can be found between Oberrieden and Richterswil, where the maximum inundation distance reaches up to ~ 200 m, with flow depths exceeding 1 m mostly in the shore-proximal zones. The eastern shores of the deep basin show the highest flow depths, mostly in the range between

Fig. 6 Time series of wave amplitudes at different gauges for hypothetical landslides caused by an earthquake with a median PGA expected for an EP_{50} of 10% (a) and 2% (b)



1 and 4 m. Most parts of the island of Lützelau would be inundated (Fig. 9).

5 Discussion

5.1 Quality and limitations of the applied model

The results of this study, i.e. the modelled wave heights and inundation, are based on various steps involving

mapping, modelling, and interpretation. Each of these steps involves limitations and uncertainties, which are difficult to assess. Therefore, the results presented here can be considered as first-order results.

5.1.1 Mapped past and potential future translational areas

The mapped extents of the translation areas corresponding to the ~ 2210 cal. year BP event may include some uncertainties, mostly due to overprinting by gullies and

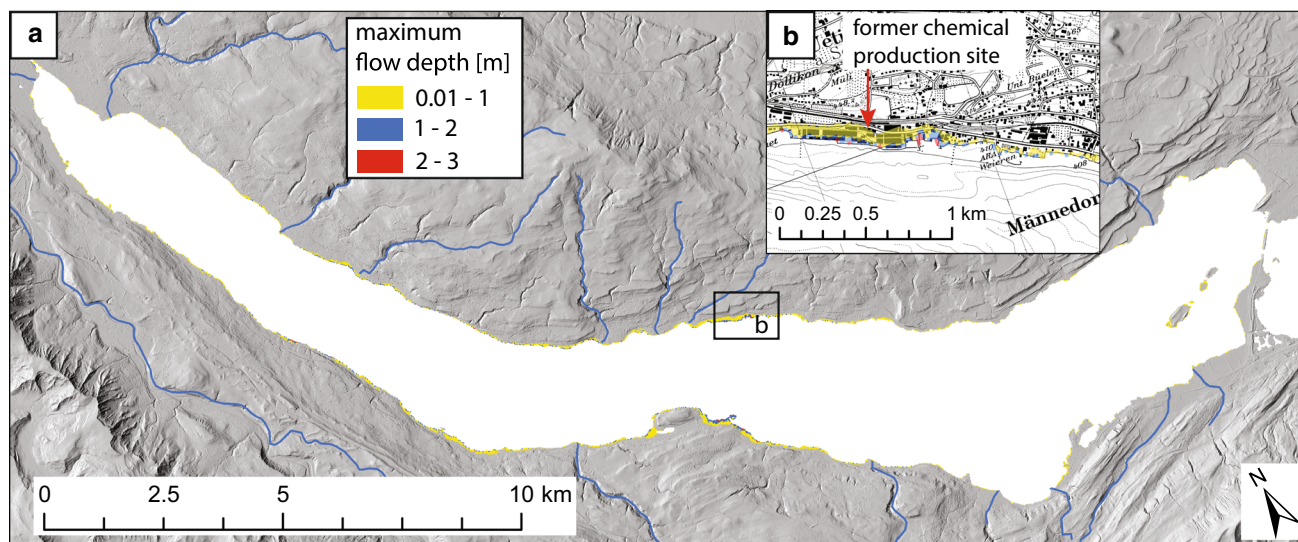


Fig. 7 Inundated areas for a tsunami as a consequence of an earthquake with a median PGA of an EP_{50} of 2%. **a** Entire lake **b** Zoom Uetikon

younger slide events (Strupler et al. 2015). However, in general, there is a relatively good agreement between the runout distances and areas of the modelled and mapped mass transport deposits. As a first simplification from the probabilistic assessment of the earthquake-triggered subaqueous landslide hazard, Strupler et al. (2018) arbitrarily considered all slopes with a failure probability of > 0.6 to fail for each hazard scenario. Also, the approach of using constant earthquake acceleration as input in the pseudo-static analysis in the study of Strupler et al. (2018) showed its limitation, especially for high earthquake accelerations, such as the ~ 0.2 g representing an earthquake with a return period of 9975 years in the study area, which would cause failure even on slopes with gradients $< 1^\circ$. In this study, slopes $< 1^\circ$ were considered stable here, to avoid large instable volumes on the terraces of the escarpment structure. However, it needs to be tested if the slope-stability assessment of Strupler et al. (2017) is valid for the lateral slopes only or if it also applies for the escarpment structure.

5.1.2 Mobility analysis

The back-analysed subaqueous landslides modelled as a Bingham fluid may not represent the mechanism of translational subaqueous landslides correctly, as the modelled slides do not actually glide, but rather flow. However, Hilbe and Anselmetti (2015) showed that the resulting landslide-triggered tsunami wave height compared relatively well to historical reports of wave heights and inundation, indicating that the model provides realistic results.

The fact that rheological parameters were back-analysed on the ~ 2210 cal. year BP Oberrieden slide and used for the simulation of all scenarios may ignore varying

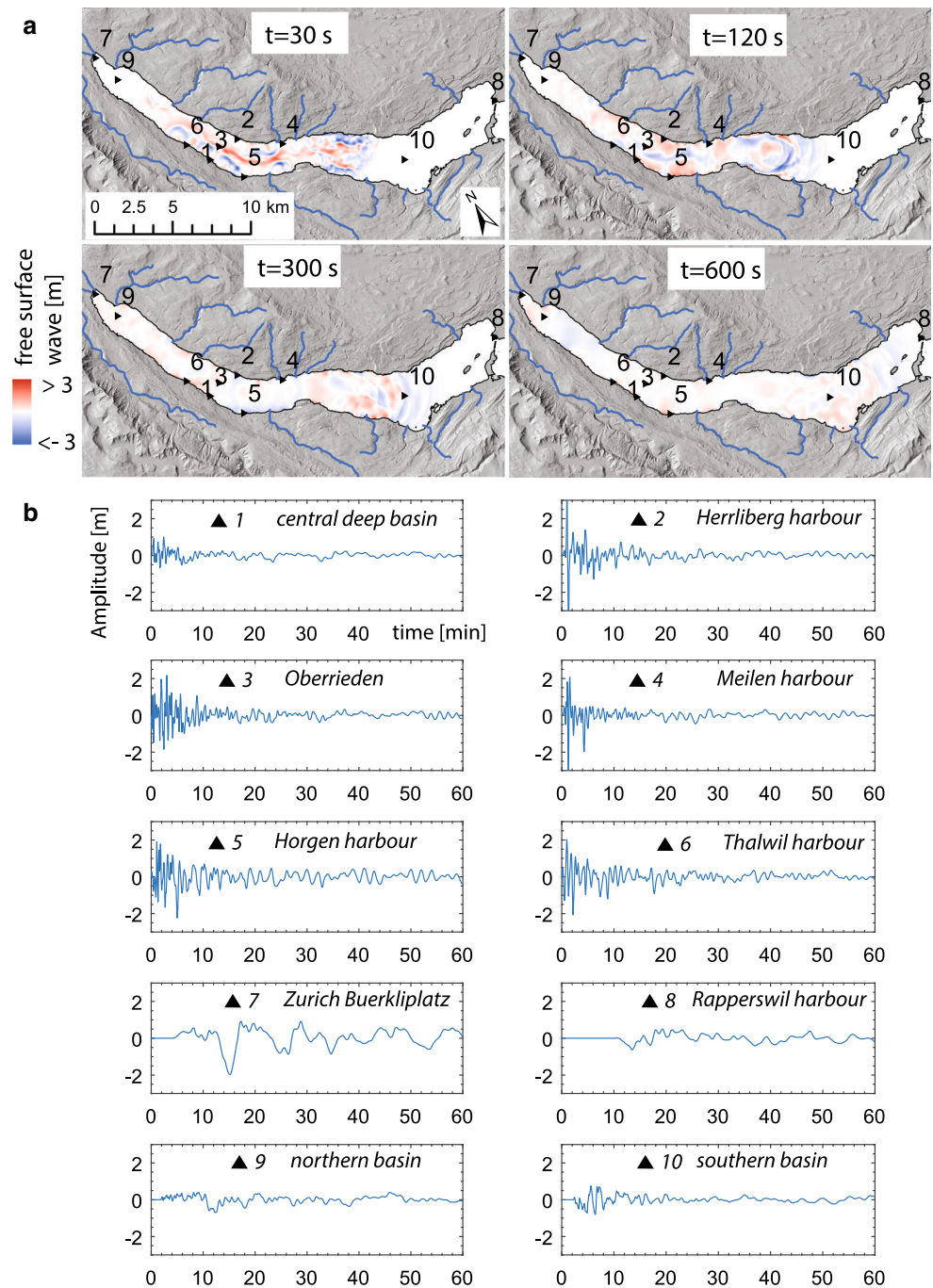
sediment-mechanical and geomorphic influences on the slide velocities within the lateral slopes. Also, a potential dependency of the parameters on the slide volumes was not considered. However, the modelled extents match the mapped extents of the ~ 2210 cal. year BP deposits relatively accurately, particularly on the western lateral slopes. On the eastern lateral slopes, the modelled extents are slightly smaller than the mapped extents. The comparably steeper lateral slopes on the eastern part of the basin (Strupler et al. 2015) might cause faster slide velocities and hydroplaning, which increases the runout of landslides and may cause distal turbidites (e.g. Mohrig et al. 1998; Elverhoi et al. 2010). This process, however, is not considered in the model.

A further simplification stems from the fact that no interaction with the underlying sediment occurs in the model. Compared to thicknesses of the MTDs measured in the seismic reflection dataset (Strasser et al. 2013), the modelled thicknesses of past slides are thus generally much lower. It may be tested in future work what the effect of the interaction between landslides and the underlying sediment is on the modelled tsunamis.

5.1.3 Tsunami model

A typical weakness of the applied model, i.e. the overestimation of the wave height and flow depth in the near field of tsunami sources, needs to be considered for the data interpretation (Hilbe and Anselmetti, 2015). Thus, if an area with great inundation is close to a translation area of a landslide, the results (especially high values of single cells) need to be interpreted with caution. However, the wave heights and impacts on the shore at a certain distance from the landslide are assumed to be acceptably approximated.

Fig. 8 Plotted time steps of wave amplitudes **a** and time series at the different gauges **b** for the hypothetical ‘worst case scenario’ of landslides occurring on all yet unfailed slopes (scenario for earthquake median PGA expected for an EP_{50} of 0.5%). Expected time of arrival of the first wave at the northern end of the lake is ~ 5 min (gauge 7) and at the southern end ~ 12 min (gauge 8)



As the height of the wave is mainly depending on the slide volumes, speed and depth of submergence (Watts 1998), uncertainties in these parameters contribute to the uncertainties in the tsunami height. The estimated cumulative volumes of all slides occurring coevally represent a worst-case scenario, thus maximum expected wave heights. Also, the scenarios modelled here all assume that sliding occurred at once, i.e. not retrogressively in multiple phases, as documented for the anthropogenically triggered Horgen slide (Heim 1876; Kelts and Hsü 1980). Sliding in multiple

phases would result in smaller individual slide volumes, reducing the resulting tsunami wave height. The landslide hazard map (Strupler et al. 2018) does not consider retrogressive failure implying that the volumes assumed to fail are derived from mapped zones with a high PoF_{co} . However, because geomorphic data shows that most of the slides in Lake Zurich are initiated immediately at the upper end of a steep zone (Strupler et al. 2015), the mapped slides can be assumed to represent potential slide extents. Also, a potential retrogressive slide mechanism may be slower

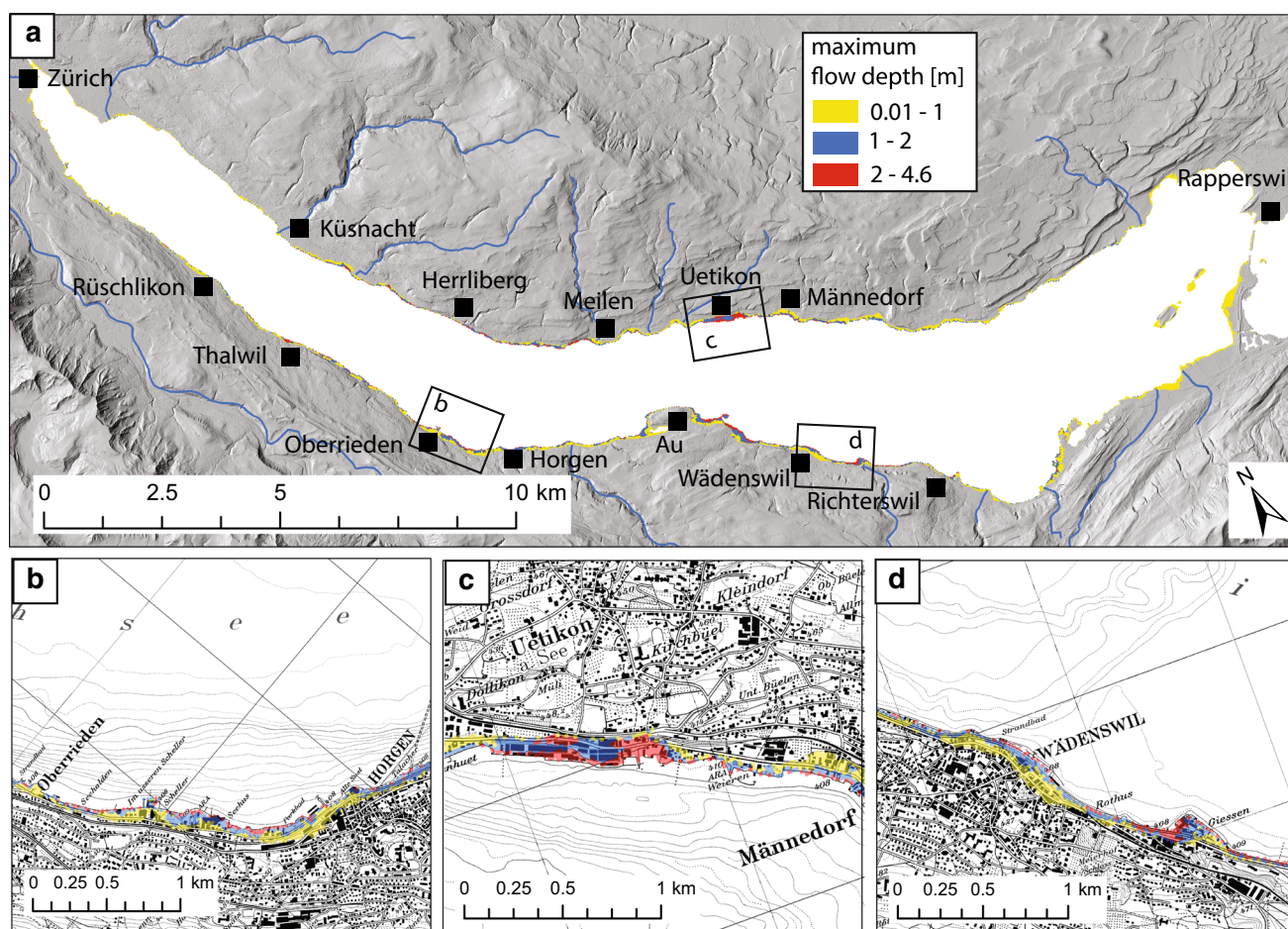


Fig. 9 Inundated areas with color-coded flow depth estimated for landslides triggered by an earthquake with an EP_{50} of 0.5% ('worst case scenario'). **a** Overview map of the whole study area. **b** Oberrieden, **c** Uetikon, **d** Wädenswil

than failure initiating at the top of the slope, which would result in lower initial wave elevations (Tappin 2017).

The inundation area is strongly affected by the surface roughness represented by houses and other infrastructure (e.g. Shimazu 2016), which have been neglected in our approach. The arbitrary selection of a Manning roughness coefficient that is lower than values typically used for built-up areas, thus leads to an overestimation of the inundation area. Using a digital surface model that includes buildings and trees that limit inundated zones and using a significantly higher spatial resolution of the inundated area might be needed for a better prediction of inundated zones. However, the first assessment of potential tsunamis generated by earthquake-triggered landslides for Lake Zurich presented here provides a first-order overview on which areas may be exposed to a tsunami hazard (and which areas may be less exposed). By assuming a 2 m higher lake level for the investigation of tsunami scenarios ~ 2210 cal. year BP, the inundation at anthropogenically designed near-shore zones might be overestimated as well, as human

activity since industrialization flattened the shore morphology at many locations.

In summary, the first-order results presented here of wave heights and inundation provide valuable information about consequences of potential past and future tsunamis on Lake Zurich if interpreted with the necessary caution. Because of the above-mentioned factors, the results can be considered as conservative, representing worst-case scenarios.

5.2 Tsunamigenic potential of past subaqueous landslides on the lateral slopes of Lake Zurich ('paleotsunamis')

Compared to estimated volumes of past landslides for other lakes in Switzerland (up to ~ 250 Mio m^3 ; Kremer et al. 2015; Hilbe and Anselmetti 2015) the total volume of the slides assigned to ~ 2210 cal. year BP (4 Mio m^3) is rather small. The mobility analysis of the ~ 2210 cal. year BP Oberrieden slide, whose rheological parameters were

calibrated in order to match the mapped extent of the depositional lobe (Strupler et al. 2015), resulted in maximum slide speeds of ~ 14 m/s. This value lies between the velocity of the modelled slides by Hilbe and Anselmetti (2015) in Lake Lucerne (~ 20 to 35 m/s), and velocities mentioned by Kremer et al. (2015) for Lake Geneva (6 to 11 m/s). Different slide volumes, height drops and slope angles, together with the back-analysed dynamic viscosity of the slide material are likely responsible for these differences. For example, the volume of the ~ 2210 cal. year BP Oberrieden slide (~ 0.8 Mio m^3) is much smaller than the Weggis slide in Lake Lucerne (~ 11.5 Mio m^3 ; Hilbe and Anselmetti, 2015). Also its height drop is significantly lower (~ 94 vs. ~ 120 m). Additionally, we back-analysed a higher dynamic viscosity (40 vs. 8 Pa s). The confined frontal emplacement of the ~ 2210 cal. year BP Oberrieden slide, showing very distinct frontal bulges (Strupler et al. 2015) may be interpreted as a geomorphic confirmation of a rather low slide speed. In contrast, slides with higher speeds may develop hydroplaning (i.e. the front of the slides glide on a water layer; Mohrig et al. 1998) and run out of their stratigraphic position, ending up in frontally emergent slides (De Blasio 2011; Moernaut and De Batist 2011).

The tsunami simulation of the ~ 2210 cal. year BP Oberrieden slide (ESM, Figs. 2 and 3) indicates no considerable inundated areas. Apart from the initial wave trough of ~ 1.5 m and subsequent crest of ~ 1 m immediately offshore behind the slide, possibly related to an overestimation of simulated wave heights close to landslide source areas (Hilbe and Anselmetti 2015), the peak amplitude remains very low (i.e. < 0.5 m). This result also coincides with the lack of tsunami observations during the 1875 Horgen slide, which had a comparable total slide volume ($1\text{--}1.5$ Mio m^3 ; Kelts 1978). However, the Horgen slide occurred in multiple slide phases (Heim 1876; Kelts and Hsü 1980), thus with lower sliding volumes for each phase than the total volume, reducing the tsunami potential.

If all the ten documented slides that were dated to ~ 2210 cal. year BP (Strasser et al. 2013) occurred synchronously (total volume of ~ 4 Mio m^3), the zones close to the shores of today's villages of Oberrieden and Thalwil would have been affected by inundations with flow depths at single cells of up to 3 m. However, these maximum flow depths appear in the vicinity of landslide translation areas correlated to the 2210 cal. year BP event (Strasser et al. 2013; Strupler et al. 2015). Therefore (due to the previously mentioned weakness of the tsunami model) it is likely that the flow depth values in near field of tsunami sources are overestimated. The villages located around the shallower northern and southern basins are less affected by tsunamis, as the wave experiences a greater drag in shallower waters (Berger et al. 2011). We conclude that the

most slide-distal areas of the future cities of Zurich and Rapperswil were not directly affected by a potential tsunami triggered by a simultaneous failure of all the landslides assigned to a ~ 2210 cal. year BP event (Strasser et al. 2013).

Only little is known about settlements located around the deep basin at the time of the assumed ~ 2210 cal. year BP (i.e. ~ 200 B.C) earthquake, but it is assumed that the direct shorelines were not inhabited anymore, as they were earlier during lake dwellers epoch in the Neolithic and Bronze Age periods (Primas 1981; Ruoff 1981). In historical terms, the earthquake and related landslides have occurred in the La Tène epoch (~ 500 B.C to 0; Wells 2002) of the Iron age. Among the few archaeological findings along the shorelines is a grave, dated to the mid La Tène epoch, that was found in Horgen (Swiss LV03 Coordinates: 688250/234825; Fig. 5). The grave is located at 410 m a.s.l., thus only 2 m above the paleo-lake level estimated for that time (Müller et al. 1999; Wild 2009). Additional historical information on occupation gaps along the lake shores may provide helpful insight on potentially disastrous tsunamis, such as discussed in Kremer et al. (2014). These authors suggested a causal relationship between an occupation gap of lake dwellers settlements on the shores of Lake Geneva and a reconstructed tsunami event dated to 1758 BC.

Our simulations represent the 'worst-case', where all slides were triggered simultaneously. An important question is whether all the individual ~ 2210 cal. year BP slides (Strasser et al. 2013) occurred within the exactly same time (i.e. within few seconds). Some of these slides, for example, could also have been triggered by an after-shock of an earthquake event, thus a few min to days later, which cannot be distinguished within reflection seismic data resolution. In such a case, the potential wave height and inundation may have been smaller, mainly due to the smaller cumulative slide volume. However, it has to be further investigated, what the effect of multiple slides on the wave interference is.

5.3 Current Tsunami hazard from earthquake-triggered landslides in Lake Zurich

The modelled consequences of potential slope failures expected for PGAs with EP_{50} of 10, 2 and 0.5% indicate that the occurrence of future tsunamis on Lake Zurich cannot be excluded. The presented first-order results help predicting where and how much time after a potential landslide tsunami waves reach the shores of Lake Zurich, providing crucial data for measures such as potential evacuation planning.

The results of all three EP_{50} scenarios for tsunamis following earthquake-triggered landslides show that the

run-up is mainly dependent on the bathymetric features close to the shoreline (e.g. Grilli et al. 2009; De Blasio 2011). On relatively steep transitions from the nearshore area to the shore (i.e. around the central basin), the run-up is greater than in extended relatively shallow zones such as the northern and southern lake-basins (Fig. 1a). Due to their protection by extensive shallow-water areas and their distal location with respect to the tsunami sources, the cities of Zurich and Rapperswil are barely affected by tsunamis for all modelled scenarios.

The most tsunami-prone zones have a low elevation above lake level and are located around the deep basin. Most affected are the nearshore zones of the villages Thalwil, Oberrieden, Horgen, Wädenswil, Richterswil, Uetikon and Meilen. Results showed that the first wave arrives at these locations ~ 1 min after an earthquake has triggered the slides, implying a very short warning and reaction time. The peak wave amplitudes (excluding the values in the near field of tsunami source and single cells with high values, which were assessed to be unreliable; Hilbe and Anselmetti 2015) for an EP_{50} of 0.5% (~ 2 m) are twice as high as for an EP_{50} of 2% (~ 1 m), and four times higher than for an EP_{50} of 10% (~ 0.5 m), mainly as a consequence of the higher slide volumes expected for stronger earthquakes. Similarly, expected flow depths and inundation areas are also greater for earthquakes with a lower EP_{50} .

Another thing to consider is that although the lake level is also fluctuating up to ~ 1 m (AWEL 2016), a hypothetical lake level rise of ~ 1 m cannot be compared to a wave with an amplitude of ~ 1 m—for the following reasons: First, the lake level would rise much slower (i.e. hours to days), whereas a tsunami wave on Lake Zurich would arrive at the shores within seconds to minutes after being generated by a subaqueous landslide. Second, a tsunami wave of 1 m amplitude would shoal on the shore, i.e. increasing its amplitude, which would result in greater inundation areas and flow depths. Whereas for a lake-level rise, the movement of the water is only in the vertical direction, for a tsunami, there is a horizontal component in the movement of the water in the shallow areas.

Quantifying the absolute tsunami hazard caused by earthquake-triggered landslides seems difficult, as the subaqueous landslide hazard is also dependent on transient conditions of the sediment drape (e.g. Strupler et al. 2018). An earthquake with a certain return period does not automatically imply that a tsunami will occur. For example, if most of the potentially mobile sediment drape has been removed by landslides as a consequence of a strong earthquake, a subsequent earthquake with the same intensity may not cause landslides of considerable sediment volumes, and as a consequence no tsunami would occur. In contrast to simulations from Lake Geneva, where a tsunami

that was caused by a delta collapse propagated as relatively simple wave train along the lake axis (Kremer et al. 2012), the coeval slides modelled here at the lateral slopes cause interference between the waves, resulting in a complex interference pattern.

5.4 Outlook

The simulation of tsunamis generated by different hypothetical earthquake-triggered landslides allows an estimation of zones affected by tsunami impacts. Due to the more alpine-proximal setting of Lake Lucerne, its topography is more complex and thus, large parts of the shore are not inhabited. In contrast, the shores of Lake Zurich are densely inhabited. As a consequence, a potential tsunami causing a similar flow depth and inundation area may create much greater damage on the shores of Lake Zurich than of Lake Lucerne, e.g. in the Gersau-basin; Hilbe and Anselmetti (2015). A quantitative tsunami-risk analysis, based on the results presented here, would be a step towards quantifying the economic impact of potential tsunamis. To this end, as risk is defined as the product of hazard, exposure and vulnerability, additional information on the latter two factors needs to be included.

The presented tsunami hazard assessment also allows for hazard mitigation measures: Knowing which zones are endangered, the authorities could for example install an early warning system that is activated by strong earthquake and design some evacuation areas. However, the relatively short travel times of waves (due to the limited basin sizes) in lakes compared to marine settings are challenging (Kremer et al. 2015). In such cases, self-evacuation education may be the best mitigation option. Land-use planning authorities may consider the first-order results presented here for zonation.

To our knowledge, no clear evidence of paleotsunamis has been described in the geological records at the shores of Lake Zurich. The zones mapped here that would have been affected by a potential tsunami following the ~ 2210 cal. year BP event may define investigation areas for paleotsunami deposits.

6 Conclusions

In this study, we modelled the tsunamigenic potential of documented earthquake-triggered Holocene landslide events occurring on the lateral slopes of Lake Zurich. Furthermore, we presented the first assessment of tsunamis that may be triggered by future earthquake-triggered landslides at a basin-wide scale. For that purpose, we used volumes of potential landslides from a probabilistic earthquake-triggered subaqueous landslide hazard map (Strupler

et al. 2018). The presented estimated flow depths and inundation areas around the entire basin of Lake Zurich can be considered as first-order, rather conservative results. However, our results provide valuable information that may be used for a more detailed simulation at a more local level.

We conclude that a coeval occurrence of all the landslides assigned to the ~ 2210 cal. year BP earthquake event may have triggered a tsunami with peak free surface wave heights of up to ~ 1.5 m. The shorelines around the deep basin may have experienced flow depths of up to ~ 3 m. A single slide assigned to the same earthquake-event, such as the well-described Oberrieden slide, may have caused a wave with a maximum free surface height of ~ 0.5 m, and thus no serious inundations on the lakeshores. However, as the shorelines today are (due to anthropogenic activity since industrialisation) different to the ones in the past, the back-calculated inundations represent only first-order estimations.

Our modelled scenarios indicate that a tsunami hazard exists for Lake Zurich. The zones most affected by potential tsunamis are the shore-proximal zones of the villages located around the deep, central basin, especially, where the greater water depths exist close to the shore. However, a considerable tsunami hazard caused by landslides only exists for earthquakes with very low exceedance probabilities in 50 years (i.e. large return periods).

For selected landslide-hazard levels, the following consequences may be expected:

- According to our model, an earthquake with PGAs of ~ 0.05 g (as expected for an exceedance probability of 10% in 50 years, which corresponds to a mean return period of 475 years) would generate a total expected slide volume of ~ 3 Mio m³, causing waves with peak amplitudes less than 0.5 m and no considerable inundations on the shorelines of Lake Zurich.
- Expected PGAs of ~ 0.1 g (exceedance probability of 2% in 50 years, which corresponds to a mean return period of 2475 years) cause failure on most slopes steeper than $\sim 10^\circ$ (Strupler et al. 2018), leading to total slide volumes of ~ 12 Mio m³. This may cause tsunamis with peak wave amplitudes of ~ 1 m and inundations on the shores around the central basin. However, the flow depth on most of these zones is calculated to amount only to a few dm.
- A ‘worst case scenario’ of all yet unfailed slopes sliding simultaneously, that is assumed for PGAs with an exceedance period of 0.5% in 50 years (corresponding to a mean return period of 9975 years), may cause tsunami waves of up to 2 m peak free surface amplitude. Inundation can be expected on all shorelines, with greatest impact around the central basin,

where maximum flow depths of up to ~ 4.6 m and maximum inundation-distances of the water up to ~ 200 m are modelled.

The cities of Zurich and Rapperswil, located on the northern and southern ends of the lake, respectively, are assumed to experience comparably little damage, even for a worst-case scenario (i.e. simultaneous triggering of all the yet unfailed slopes), because they are protected by large, relatively shallow zones, that decelerate the tsunami wave.

Acknowledgements This work was supported by the Swiss National Foundation Grant no. 133481. K. K. is currently funded by the Swiss National Science Foundation (Project number PMPDP2_171318). Swisstopo geodata was reproduced with the authorisation (JA100120). We would like to thank the developers of MassMov2D and GeoClaw for providing the open-source codes.

References

- AWEL (2016) Wasserstand Zürichsee—Oberrieden 2010-2016. <http://www.hw.zh.ch/hochwasser/jahrbuch/0502w016.PDF>. Accessed 16 Apr 2017
- Beguería, S., Van Asch, T. W. J., Malet, J.-P., & Gröndahl, S. (2009). A GIS-based numerical model for simulating the kinematics of mud and debris flows over complex terrain. *Natural Hazards and Earth Systems Sciences*, 9, 1897–1909. <https://doi.org/10.5194/nhess-9-1897-2009>.
- Berger, M. J., George, D. L., LeVeque, R. J., & Mandli, K. T. (2011). The GeoClaw software for depth-averaged flows with adaptive refinement. *Advances in Water Resources*, 34, 1195–1206. <https://doi.org/10.1016/j.advwatres.2011.02.016>.
- Bondevik, S., Løvholt, F., Harbitz, C., Mangerud, J., Dawson, A., & Svendsen, J. I. (2005). The storegga slide tsunami—comparing field observations with numerical simulations. *Marine and Petroleum Geology*, 22, 195–208. <https://doi.org/10.1016/j.marpetgeo.2004.10.003>.
- Bornhold, B. D., & Thomson, R. E. (2012). Tsunami hazard assessment related to slope failures in coastal waters. In J. J. Clague & D. Stead (Eds.), *Landslides* (pp. 108–120). Cambridge: Cambridge University.
- Bretschneider CL and Wybro PG (1977) Tsunami inundation prediction. In: Proceedings of the Fifteenth coastal Engineering Conference. Am. Soc. of Civil Engineers, New York, p 1006–1024
- De Blasio, F. V. (2011). Subaqueous Landslides. *Introduction to the Physics of Landslides* (pp. 295–351). Netherlands: Springer.
- Elverhoi, A., Breien, H., De Blasio, F. V., Harbitz, C. B., & Pagliardi, M. (2010). Submarine landslides and the importance of the initial sediment composition for run-out length and final deposit. *Ocean Dynamics*, 60, 1027–1046. <https://doi.org/10.1007/s10236-010-0317-z>.
- Fine, I. V., Rabinovich, A. B., Bornhold, B. D., Thomson, R. E., & Kulikov, E. A. (2005). The Grand Banks landslide-generated tsunami of November 18, 1929: preliminary analysis and numerical modeling. *Marine Geology*, 215, 45–57. <https://doi.org/10.1016/j.margeo.2004.11.007>.
- Geilinger-Schnorf U (1993) 175 Jahre Chemie Uetikon: Die Geschichte der Chemischen Fabrik Uetikon von 1818 bis 1993. UBV Uetikon Betriebs- und Verwaltungs-AG, Uetikon
- Grilli, S. T., Taylor, O. D. S., Baxter, C. D. P., & Marezki, S. (2009). A probabilistic approach for determining submarine landslide

- tsunami hazard along the upper east coast of the United States. *Marine Geology*, 264, 74–97. <https://doi.org/10.1016/j.margeo.2009.02.010>.
- Harbitz, C. B. (1992). Model simulations of tsunamis generated by the Storegga Slides. *Marine Geology*, 105, 1–21. [https://doi.org/10.1016/0025-3227\(92\)90178-K](https://doi.org/10.1016/0025-3227(92)90178-K).
- Heim, A. (1876). Bericht und Expertengutachten über die im Februar und September 1875 in Horgen am Zürichsee vorgekommenen Rutschungen. *Die Eisenbahn*, 4, 191–196.
- Henriod S, Douard R, Ullmann D and Humbel R (2016) Statistik der Bevölkerung und Haushalte (STATPOP). Bundesamt für Statistik (BFS), Bern. BFS-Nummer: be-d-00.03-13-STATPOP-v16
- Hilbe, M., & Anselmetti, F. S. (2015). Mass Movement-Induced Tsunami Hazard on Perialpine Lake Lucerne (Switzerland): scenarios and Numerical Experiments. *Pure and Applied Geophysics*, 172, 545–568. <https://doi.org/10.1007/s00024-014-0907-7>.
- Hill, J., Collins, G. S., Avdis, A., Kramer, S. C., & Piggott, M. D. (2014). How does multiscale modelling and inclusion of realistic palaeobathymetry affect numerical simulation of the Storegga Slide tsunami? *Ocean Modelling*, 83, 11–25. <https://doi.org/10.1016/j.ocemod.2014.08.007>.
- Intergovernmental Oceanographic Commission (2016) Tsunami Glossary. IOC Technical Series 85. UNESCO, Paris
- Jiang, L., & Leblond, P. H. (1992). The Coupling of A Submarine Slide and The Surface. *Journal of Geophysical Research*, 97, 12731–12744.
- Kaiser, G., Scheele, L., Kortenhaus, A., Løvholt, F., Römer, H., & Leschka, S. (2011). The influence of land cover roughness on the results of high resolution tsunami inundation modeling. *Natural Hazards and Earth Systems Sciences*, 11, 2521–2540. <https://doi.org/10.5194/nhess-11-2521-2011>.
- Keller, O., & Krayss, E. (2005). Der Rhein-Linthe-Gletscher im letzten Hochglazial. 1. Teil: einleitung, Aufbau und Abschmelzen des Rhein-Linthe-Gletschers im Oberen Würm. *Verteljahrsschrift der Naturforschenden Gesellschaft Zürich*, 150, 19–32.
- Kelts K (1978) Geological and sedimentary evolution of Lakes Zurich and Zug, Switzerland. ETH Zurich, PhD Thesis, Nr.6146
- Kelts, K., & Hsü, K. J. (1980). Resedimented facies of 1875 Horgen slumps in Lake Zurich and a process model of longitudinal transport of turbidity currents. *Eclogae Geologicae Helveticae*, 73, 271–281.
- Kremer, K., Hilbe, M., Simpson, G., Decrouy, L., Wildi, W., & Girardclos, S. (2015). Reconstructing 4000 years of mass movement and tsunami history in a deep peri-Alpine lake (Lake Geneva, France-Switzerland). *Sedimentology*. <https://doi.org/10.1111/sed.12190>.
- Kremer, K., Marillier, F., Hilbe, M., Simpson, G., Dupuy, D., Yrro, B. J. F., et al. (2014). Lake dwellers occupation gap in Lake Geneva (France–Switzerland) possibly explained by an earthquake–mass movement–tsunami event during Early Bronze Age. *Earth and Planetary Science Letters*, 385, 28–39. <https://doi.org/10.1016/j.epsl.2013.09.017>.
- Kremer K, Simpson G, Girardclos S (2012) Giant Lake Geneva tsunami in ad 563. 5:2011–2013.
- Kuen E (1999) Der Uferabbruch im Kusén. In: Künsbacher Jahrheft. Ortsgehistorische Kommission der Kulturellen Vereinigung Künsnacht, p 44–50
- Lee H, Schwab W, Booth J (1993) Submarine landslides: an introduction. In: Schwab WC, Lee HJ, Twichell DC (eds) Submarine landslides: selected studies in the US exclusive economic zone. US Geological Survey Bulletin 2002, p 1–11
- Locat, J., & Lee, H. J. (2002). Submarine landslides: advances and challenges. *Canadian Geotechnical Journal*, 39, 193–212. <https://doi.org/10.1139/t01-089>.
- López-Venegas, A. M., ten Brink, U. S., & Geist, E. L. (2008). Submarine landslide as the source for the October 11, 1918 Mona Passage tsunami: observations and modeling. *Marine Geology*, 254, 35–46. <https://doi.org/10.1016/j.margeo.2008.05.001>.
- Løvholt, F., Harbitz, C. B., & Haugen, K. B. (2005). A parametric study of tsunamis generated by submarine slides in the Ormen Lange/Storegga area off western Norway. *Marine and Petroleum Geology*, 22, 219–231. <https://doi.org/10.1016/j.marpetgeo.2004.10.017>.
- Mei, C. C., & Liu, K.-F. F. (1987). A Bingham-plastic model for A muddy seabed under long waves. *Journal of Geophysical Research*, 92, 14581–14594. <https://doi.org/10.1029/JC092iC13p14581>.
- Moernaut, J., & De Batist, M. (2011). Frontal emplacement and mobility of sublacustrine landslides: results from morphometric and seismostratigraphic analysis. *Marine Geology*, 285, 29–45. <https://doi.org/10.1016/j.margeo.2011.05.001>.
- Mohrig, D., Whipple, K. X., Hondzo, M., Ellis, C., & Parker, G. (1998). Hydroplaning of subaqueous debris flows. *Bulletin of the Geological Society of America*, 110, 387–394. [https://doi.org/10.1130/0016-7606\(1998\)110<0387:HOSDF>2.3.CO;2](https://doi.org/10.1130/0016-7606(1998)110<0387:HOSDF>2.3.CO;2).
- Müller, F., Kaenel, G., & Lüscher, G. (1999). *Eisenzeit = Age du Fer. Die Schweiz vom Paläolithikum bis zum frühen Mittelalter. SPM IV*. Basel: Schweizerische Gesellschaft für Ur- und Frühgeschichte.
- Nipkow F (1927) Über das Verhalten der Skelette planktischer Kieselalgen im geschichteten Tifenschlamm des Zürich- und Baldeggensees. ETH Zurich, PhD Thesis, Nr. 455
- Pararas-Carayannis, G. (1988). Risk assessment of the tsunami hazard. In M. I. El-Sabh & T. S. Murty (Eds.), *Natural and man-made hazards* (pp. 183–191). Dordrecht: Springer.
- Pelinovsky, E. N., & Mazova, R. K. (1992). Exact analytical solutions of nonlinear problems of tsunami wave run-up on slopes with different profiles. *Natural Hazards*, 6, 227–249. <https://doi.org/10.1007/BF00129510>.
- Primas M (1981) Urgeschichte des Zürichseegebietes im Überblick: Von der Steinzeit bis zur Früheisenzeit. In: Degen R (ed) Zürcher Seeufersiedlungen—Von der Pfahlbau-Romantik zur modernen archäologischen Forschung (pp. 5–18). Basel: Schwabe.
- Reusch, A., Moernaut, J., Anselmetti, F. S., & Strasser, M. (2016). Sediment mobilization deposits from episodic subsurface fluid flow—A new tool to reveal long-term earthquake records? *Geology*, 44, 243–246. <https://doi.org/10.1130/G37410.1>.
- Ruoff U (1981) Die Ufersiedlungen a Zürich- und Greifensee. In: Degen R (ed) Zürcher Seeufersiedlungen—Von der Pfahlbau-Romantik zur modernen archäologischen Forschung (pp. 19–61). Basel: Schwabe.
- Schlund RA (1972) Zürichsee: topogr. Plan 1:5000. Meliorations- und Vermessungsamt des Kt. Zürich.
- Schnellmann, M., Anselmetti, F. S., Giardini, D., McKenzie, J. A., & Ward, S. N. (2002). Prehistoric earthquake history revealed by lacustrine slump deposits. *Geology*, 30, 1131–1134. [https://doi.org/10.1130/0091-7613\(2002\)030<1131:PEHRBL>2.0.CO;2](https://doi.org/10.1130/0091-7613(2002)030<1131:PEHRBL>2.0.CO;2).
- Shimazu, H. (2016). Relationships between coastal and fluvial geomorphology and inundation processes of the tsunami flow caused by the 2011 off the pacific coast of tohoku earthquake. *Natural disaster and coastal geomorphology* (pp. 65–92). Cham: Springer.
- Siegenthaler, C., Finger, W., Kelts, K., & Wang, S. (1987). Earthquake and seiche deposits in Lake Lucerne, Switzerland. *Eclogae Geologicae Helveticae*, 80, 241–260.
- Skvortsov, A., & Bornhold, B. (2007). Numerical simulation of the landslide-generated tsunami in Kitimat Arm, British Columbia, Canada, 27 April 1975. *Journal of Geophysical Research: Earth Surface*, 112, 1–12. <https://doi.org/10.1029/2006JF000499>.

- Strasser, M., Monecke, K., Schnellmann, M., & Anselmetti, F. S. (2013). Lake sediments as natural seismographs: a compiled record of Late Quaternary earthquakes in Central Switzerland and its implication for Alpine deformation. *Sedimentology*, *60*, 319–341. <https://doi.org/10.1111/sed.12003>.
- Strasser, M., Schindler, C., & Anselmetti, F. S. (2008). Late Pleistocene earthquake-triggered moraine dam failure and outburst of Lake Zurich, Switzerland. *Journal of Geophysical Research: Earth Surface*, *113*, 1–16. <https://doi.org/10.1029/2007JF000802>.
- Strupler, M., Danciu, L., Hilbe, M., Kremer, K., Anselmetti, F. S., Strasser, M., et al. (2018). A subaqueous hazard map for earthquake-triggered landslides in Lake Zurich, Switzerland. *Natural Hazards*, *90*, 51–78. <https://doi.org/10.1007/s11069-017-3032-y>.
- Strupler, M., Hilbe, M., Anselmetti, F. S., Kopf, A. J., Fleischmann, T., & Strasser, M. (2017). Probabilistic stability evaluation and seismic triggering scenarios of submerged slopes in Lake Zurich (Switzerland). *Geo-Marine Letters*, *37*, 241–258. <https://doi.org/10.1007/s00367-017-0492-8>.
- Strupler, M., Hilbe, M., Anselmetti, F. S., & Strasser, M. (2015). Das neue Tiefenmodell des Zürichsees: hochauflösende Darstellung der geomorphodynamischen Ereignisse im tiefen Seebecken. *Swiss Bulletin für Angewandte Geologie*, *20*, 71–83.
- Synolakis, C. E., Bardet, J.-P., Borrero, J. C., Davies, H. L., Okal, E. A., Silver, E. A., et al. (2002). The slump origin of the 1998 Papua New Guinea Tsunami. *Proceedings of the Royal Society of London A: Mathematical, Physical and Engineering Sciences*, *458*, 763–789. <https://doi.org/10.1098/rspa.2001.0915>.
- Tappin, D. R. (2017). The generation of tsunamis. *Encyclopedia of maritime and offshore engineering* (pp. 1–10). Chichester: Wiley.
- Tappin, D. R., Matsumoto, T., Watts, P., Satake, K., McMurtry, G. M., Matsuyama, M., et al. (1999). Sediment slump likely caused 1998 Papua New Guinea Tsunami. *Eos (Washington DC)*. <https://doi.org/10.1029/99EO00241>.
- Tappin, D. R., Watts, P., & Grilli, S. T. (2008). The Papua New Guinea tsunami of 17 July 1998: anatomy of a catastrophic event. *Natural Hazards and Earth Systems Sciences*, *8*, 243–266.
- Tappin, D. R., Watts, P., McMurtry, G. M., Lafoy, Y., & Matsumoto, T. (2001). The Sissano, Papua New Guinea tsunami of July 1998—Offshore evidence on the source mechanism. *Marine Geology*, *175*, 1–23. [https://doi.org/10.1016/S0025-3227\(01\)00131-1](https://doi.org/10.1016/S0025-3227(01)00131-1).
- ten Brink, U. S., Lee, H. J., Geist, E. L., & Twichell, D. (2009). Assessment of tsunami hazard to the US East Coast using relationships between submarine landslides and earthquakes. *Marine Geology*, *264*, 65–73. <https://doi.org/10.1016/j.margeo.2008.05.011>.
- Tinti, S., & Bortolucci, E. (2000). Energy of water waves induced by submarine landslides. *Pure and Applied Geophysics*, *157*, 281–318. <https://doi.org/10.1007/s000240050001>.
- Wang, X., Mountjoy, J., Power, W. L., & Lane, E. M. (2016). *Coupled modelling of the failure and tsunami of a submarine debris avalanche offshore Central New Zealand*. Cham: Springer.
- Ward, S. N. (2011). Tsunami. In H. K. Gupta (Ed.), *Encyclopedia of solid earth geophysics* (pp. 1473–1493). Dordrecht: Springer.
- Watts, P. (1998). Wavemaker curves for tsunamis generated. *Journal of Waterway, Port, Coastal, and Ocean Engineering*, *124*, 127–137.
- Wells, P. S. (2002). The iron age. In S. Milisauskas (Ed.), *European prehistory: A survey* (pp. 335–383). Boston: Springer.
- Wesseling, C. G., Karssenbergh, D.-J., Burrough, P., & Van Deursen, W. P. A. (1996). Integrating dynamic environmental models in GIS: the development of a dynamic modelling language. *Trans GIS*, *1*, 40–48. <https://doi.org/10.1111/j.1467-9671.1996.tb00032.x>.
- Wiemer S, Danciu L, Edwards B, Marti M, Fäh D, Hiemer S, Wössner J, Cauzzi C, Kästli P and Kremer K (2016) *Seismic hazard model 2015 for Switzerland* (pp. 1–163). Zurich: Swiss Seismological Service (SED) at ETH Zurich.
- Wild, D. (2009). Lindenhof, Sihl und Zürichsee-Fragen zu Geologie und Topographie zwischen Spätlatène und Frühmittelalter. *Zürich in der Spätlatène- und frühen Kaiserzeit—Vom keltischen Oppidum zum römischen Vicus Turicum* (pp. 14–17). Zürich: Hochbaudepartment der Stadt Zürich.